Pionic Hydrogen

D. Gotta[1], F. Amaro[2], D. F. Anagnostopoulos[3], S. Biri[4], D. S. Covita[2], H. Gorke[1], A. Gruber[5], M. Hennebach[1,8], A. Hirtl[5], T. Ishiwatari[5], P. Indelicato[6], Th. Jensen[6,9], E.-O. Le Bigot[6], J. Marton[5], M. Nekipelov[1], J. M. F. dos Santos[2], S. Schlesser[6], Ph. Schmid[5], L. M. Simons[7], Th. Strauch[1], M. Trassinelli[6,10], J. F. C. A. Veloso[2], and J. Zmeskal[5]

[1] Institut für Kernphysik, Forschungszentrum Jülich, D-52425 Jülich, Germany d.gotta@fz-juelich.de
[2] Department of Physics, Coimbra University, P-3000 Coimbra, Portugal
[3] Department of Material Science and Engineering, University of Ioannina, Ioannina, GR-45110, Greece
[4] Institut of Nuclear Research, Hungarian Academy of Sciences, H-4001 Debrecen, Hungary
[5] Stefan Meyer Institut, Austrian Academy of Sciences, A-1090 Vienna
[6] Laboratoire Kastler Brossel, UPMC-Paris 6, ENS, CNRS; Case 74, 4 place Jussieu, 75005 Paris, France
[7] Paul Scherrer Institut, Villigen PSI, CH-5232 Villigen, Switzerland
[8] WTI GmbH, D-52428 Jülich, Germany (present address)
[9] Ringkjøbing Gymnasium, Vasevej 24, 6950 Ringkjøbing, Danmark (present address)
[10] Gesellschaft für Schwerionenforschung, Plankstr. 1, D-64291, Darmstadt, Germany (present address)

Abstract. Strong-interaction shift ε_{1s} and broadening Γ_{1s} in the pionic hydrogen atom are determined from the energies and line widths of X-ray transitions to the $1s$ ground state. They are directly connected to the πN scattering lengths which are related to the πN coupling constant and the πN *sigma* term being a measure of chiral symmetry breaking. Therefore, the measurement of the pion–nucleon s-wave scattering lengths constitutes a high-precision test of the methods of chiral perturbation theory (χPT), which is the low-energy approach of QCD. Additional constraints for the πN scattering lengths are obtained from the measurement of the ground-state shift in pionic deuterium. The hadronic width is linked to s-wave pion production in nucleon–nucleon collisions. A new experiment, set up at the Paul Scherrer Institut (PSI), has finished taking data recently and will allow the determination of the scattering lengths at the few per cent level.

1 Introduction

Quantum chromodynamics (QCD) is today's microscopic theory of strong interaction based on colored fermions – the quarks – and colored massless spin

D. Gotta et al.: *Pionic Hydrogen*, Lect. Notes Phys. **745**, 165–185 (2008)
DOI 10.1007/978-3-540-75479-4_10

one-field quanta – the gluons. At highest energies, perturbative methods are applied with great success because of the decreasing strength of the interaction as described by a running strong coupling constant α_s (asymptotic freedom). At low energies, in the non-perturbative regime, a new framework – *chiral perturbation theory* (χPT) – has been proposed [1], which exploits the left–right symmetry of the QCD Lagrangian in an *ideal world* of 2 (or 3) massless light quarks u, d (and s) (chiral limit). Here *chirality* is conserved forever and pions become stable and even massless. In the *real world* chiral symmetry of the strong force is explicitly broken because of finite masses of about 3, 5 and 95 MeV/c^2 for the u, d and s quark [2]. Such small (current) quark masses are, however, unable to explain the masses of the hadron multiplets.

The weak decay of pseudoscalar (0^-) fields like pions corresponds to the non-conservation of the axial charge hiding the chiral symmetry. It results in a non-zero expectation value $B = \mid \langle 0 \mid \bar{q}q \mid 0 \rangle \mid$ (chiral condensate) of $q\bar{q}$ states between the QCD vacuum (spontaneous chiral symmetry breaking). This fact is known from current algebra as partially conserved axial current (PCAC) [3, 4]. Furthermore, neutron decay can be regarded as the strong decay $n \to p\pi^-$ and subsequent pion disintegration which connects the strong πN coupling constant $f_{\pi N}$, the weak pion decay constant F_π and the weak axial coupling g_A by $f_{\pi N} = m_{\pi^\pm} g_A / 2F_\pi$ (Goldberger–Treiman relation [5]). A comprehensive discussion is given, e. g., in [6].

Spontaneous symmetry breaking leads mandatorily to eight massless pseudoscalar particles (Goldstone bosons) which may be identified with the 0^- meson octet (π, K, η). Finite masses of these pseudoscalar mesons, though well below the usual hadronic scale of 1 GeV/c^2, especially in the case of pions, require both finite current quark mass values and a non-vanishing chiral condensate. In lowest order their masses are given by the Gell-Mann–Oakes–Renner relations [7]. For the case of pions, e. g., $m_\pi^2 = \frac{1}{2}(m_u + m_d)B/F_\pi^2 +$ higher orders. The chiral condensate, equal for all pseudoscalar mesons, adjusts the physical masses of the pseudoscalar octet. The parameters B and F_π are principally calculable within lattice QCD, but precise values still must be determined from experiment. An introduction to the concepts describing the structure of hadrons and the methods of χPT may be found elsewhere [8, 9, 10].

Approaching the chiral limit, degrees of freedom are field quanta like pions, to be described by the methods of field theory. Their interaction with (hadronic) matter can be regarded as a kind of residual interaction of QCD and is strongly influenced by the underlying chiral symmetry. On the strong-interaction scale corresponding to about the nucleon's mass, the zero mass limit is closely approached considering light mesons like the pion because of $(m_\pi / M_p)^2 \approx 2\% \ll 1$. Therefore, a perturbative approach within an effective field theory (χPT) becomes possible [1, 11, 12, 13] where symmetry properties of the QCD Lagrangian manifest in observables by means of low-energy theorems. A (chiral) expansion ordered by counting the powers of (small) momenta, the quark mass difference $(m_d - m_u)$ and the fine structure constant

α allows to include on the same footing strong isospin breaking effects resulting from the mass difference ($m_d \neq m_u$) and those of electromagnetic origin. The unknown structure of QCD at short distances is parameterized by so-called low-energy constants (LECs) and, disregarding future lattice QCD calculations, must be taken from experiment.

According to its origin, χPT works best for the lightest quarks u and d as combined in the lightest strongly interacting particle – the pion – and for the description of the pion–pion interaction [14, 15]. The experimental approach, however, is very demanding [16, 17]. On the other hand, it has been shown that such an approach can also be applied to the meson–nucleon case, then often denoted as *Heavy Baryon Chiral Perturbation Theory* (HBχPT) [9, 10, 13, 18, 19].

So called *sigma terms* represent the contribution from the finite quark masses to a baryon's mass. Applied, e.g., to the proton and u and d quarks the resulting πN σ term $\sigma_{\pi N} = \frac{1}{2}(m_u + m_d) \mid \langle p \mid \bar{q}q \mid p \rangle \mid$ measures that contribution from the quark–antiquark pairs $u\bar{u} + d\bar{d}$ at the (unphysical) Cheng–Dashen point $s - u = 0,\ t = 2m_\pi^2$ (s, t, u are the Mandelstam variables). Though located outside the physical region, *sigma terms* are related to observables by extrapolation of meson–baryon amplitudes into the unphysical region. Hence, scattering lengths are of great importance because they represent the closest approach in the real world. When comparing the result of the extrapolation to the HBχPT result, $\sigma_{\pi N}$ is sensitive to the $\bar{s}s$ contents of the nucleon [20, 21].

Exotic atoms provide an ideal laboratory to study the low-energy strong meson–baryon interaction without the need of any extrapolation to threshold because relative energies are restricted to the keV range [22]. The experiment described here aims at a precise determination of the hadronic shift ε_{1s} and broadening Γ_{1s} by measuring the transition energies and line widths of the K X-radiation from pionic hydrogen (πH) [23] in order to extract the πN scattering lengths to an accuracy of a few per cent. Further constraints will be achieved by a similar measurement of pionic deuterium (πD) [24].

At first, relations between scattering lengths, pionic atom observables and mechanisms of formation and de-excitation of pionic-hydrogen atoms are outlined. The measurement strategy is introduced followed by a short description of the experimental approach. Results achieved in earlier measurements and preliminary ones of this experiment are briefly discussed.

2 Pion–Nucleon Interaction at Threshold

Pions and nucleons combine to isospin 1/2 or 3/2 systems. For the two parameters one may choose the isoscalar and isovector scattering lengths a^+ and a^-, which are given by the isospin combinations $a^+ = (a_{1/2} + 2a_{3/2})/3$ and $a^-(a_{1/2} - a_{3/2})/3$ or in terms of the elastic reactions by $a^\pm = (a_{\pi^- p \to \pi^- p} \pm$

$a_{\pi^+p\to\pi^+p})/2$. In the limit of isospin conservation, the elastic channels are related to charge exchange by the isospin triangle, $a_{\pi^-p\to\pi^-p} - a_{\pi^+p\to\pi^+p} = -\sqrt{2}\,a_{\pi^-p\to\pi^\circ n}$. Obviously, then $a_{\pi^-p\to\pi^-p} = a^+ + a^-$ and $a_{\pi^-p\to\pi^\circ n} = -\sqrt{2}\,a^-$ holds. At threshold the πN interaction is completely described by two amplitudes reducing to two (real) numbers being identified with the s-wave scattering lengths.

Approaching threshold and considering negatively charged pions only two "nuclear" channels, $\pi^-p \to \pi^-p$ and $\pi^-p \to \pi^\circ n$, and the radiative capture reaction $\pi^-p \to \gamma n$ occur. The relative strength of charge exchange and radiative capture defines the Panofsky ratio determined to $P = 1.546 \pm 0.009$ [25].

The leading order result (LO) for a^+ and a^- derived from current algebra [26, 27] already revealed an important feature of the underlying chiral symmetry – the vanishing of the isoscalar combination a^+ in the chiral limit $a^+ = 0$ and $a^- = -0.079/m_\pi$. Deviations from these values are due to higher orders of the chiral expansion and should be small.

Within χPT a^+ and a^- are pure QCD quantities and, therefore, substantial effort is undertaken to elaborate the corrections to relate the experimentally accessible quantities to a^+ and a^- [28, 29, 30, 31, 32, 33, 34]. The πN sigma term is determined by extrapolation of the amplitude a^+ to the Cheng–Dashen point. The πN coupling constant $f^2_{\pi N}/4\pi$ is related to a^- by dispersion relation methods (Goldberger–Miyazawa–Oehme sum rule [35]). The higher orders to be calculated by χPT are obtained by comparison with the current algebra result $f^2_{\pi N,\mathrm{LO}}/4\pi = 0.072$ (Goldberger–Treiman discrepancy Δ_{GT}) and are expected to be of the order of 2% [9, 10].

Access to the πN scattering lengths a^+ and a^- and $a_{\pi D}$ is given by

- Analysis of scattering data extrapolated to threshold
- Hadronic level shift $\varepsilon^{\pi H}_{1s}$ and broadening $\Gamma^{\pi H}_{1s}$ in pionic hydrogen as well as $\varepsilon^{\pi D}_{1s}$ in pionic deuterium.

In the limit of charge symmetry, $a_{\pi^-n\to\pi^-n} = a_{\pi^+p\to\pi^+p}$ holds. Then the isoscalar scattering length is also represented by $a^+ = (a_{\pi^-p\to\pi^-p} + a_{\pi^-n\to\pi^-n})/2$ which may be regarded as pion–deuteron scattering in the limit of a scattering on a free proton and neutron. To achieve the πD scattering length itself multiple scattering, nuclear structure and absorption must be taken into account. Significant corrections are expected, because the sum $a_{\pi^-p\to\pi^-p} + a_{\pi^-n\to\pi^-n}$ almost vanishes and, consequently, the hadronic shift in πD must be small compared to estimates using a simple geometrical scaling with respect to πH.

In πD scattering *true* inelastic channels are open and, hence, $a_{\pi D}$ becomes a complex number. The real part $\Re\, a_{\pi D}$, i. e., $a^+ + \mathit{corrections}$ accounts for single and multiple scattering and the imaginary part $\Im\, a_{\pi D}$ for true pion absorption ($\pi^-d \to nn$) and radiative capture ($\pi^-d \to nn\gamma$). The ratio of the dominant channels $(\pi^-d \to nn)/(\pi^-d \to nn\gamma)$ was found to be $P_{\pi^-d} = 2.83 \pm 0.04$ [36]. Other channels contribute only to 0.1%.

3 Scattering Lengths and Pionic Atoms

3.1 Pionic Hydrogen

The scattering lengths of the elastic channel $a_{\pi^- p \to \pi^- p}$ and the charge-exchange reaction $a_{\pi^- p \to \pi^0 n}$ are related to the strong-interaction shift ε_{1s} and broadening Γ_{1s} by the Deser-type formulae [37, 38] with r_B being the exotic atom Bohr radius and B_{1s} the binding energy of the atomic ground state:

$$\frac{\varepsilon_{1s}}{B_{1s}} = -\frac{4}{r_B}\, a_{\pi^- p \to \pi^- p}(1+\delta_\varepsilon)\,, \tag{1}$$

$$\frac{\Gamma_{1s}}{B_{1s}} = 8\frac{q_0}{r_B}\left(1+\frac{1}{P}\right)[a_{\pi^- p \to \pi^0 n}(1+\delta_\Gamma)]^2. \tag{2}$$

In terms of the isospin odd and even amplitudes, $\varepsilon_{1s} \propto a^+ + a^-$ and $\Gamma_{1s} \propto (a^-)^2$ hold.

The quantities $\delta_{\varepsilon,\Gamma}$ represent the corrections to be applied to the experimentally determined scattering length in order to obtain pure strong-interaction quantities. Recent calculations for $\delta_{\varepsilon,\Gamma}$ performed within χPT include the corrections for isospin breaking both from the electromagnetic interaction and the light quark mass difference on the same footing $(m_d - m_u)$ [39, 40, 41, 42]. In the higher order terms of the chiral expansion further low-energy constants (LECs) appear. These constants have to be determined from experiment and not all of them are well known [39, 41]. Alternatively, a potential model [43] and phenomenological approaches [44] to $\delta_{\varepsilon,\Gamma}$ are presented, which differ substantially in the numerical values. Finally, the pionic-atom results must be consistent with the extrapolation of πN scattering data to threshold and πN phase-shift analyses [45, 46, 47].

3.2 Pionic Deuterium

In general, the complex pion-nucleus scattering length $a_{\pi A(Z,N)}$ is related to the measured shift ε_{1s} and width Γ_{1s} by the classical Deser formula [37]

$$\varepsilon_{1s} + \mathrm{i}\,\Gamma_{1s}/2 = -\,(2\alpha^3 Z^3 m_{\mathrm{red}}^2 c^4/\hbar c)\cdot a_{\pi A}, \tag{3}$$

where m_{red} is the reduced mass of the pion-nucleus system. Because of the small ratio hadronic scattering length a to Bohr radius r_B of the exotic atom $|\,a\,|\,/r_B \ll 1$, second order corrections due to strong Coulomb interference as given by Trueman's expansion [48] have been neglected up to now in view of the experimental accuracy of several per cent. Then the relations $\varepsilon_{1s} \propto \Re\, a_{\pi D}$ and $\Gamma_{1s} \propto \Im\, a_{\pi D}$ are still sufficient.

Significant effort has been undertaken and is still going on to describe the πD interaction at threshold in the framework of chiral Lagrangians [49, 50, 51, 52, 53, 54], in particular, since the large contribution of the isospin breaking corrections has been realized [55]. The leading term is proportional to a^+ and,

hence, about one order of magnitude smaller than the corrections originating from multiple scattering.

$$
\begin{aligned}
\Re a_{\pi d} &= S \;+\; D \;+\; \cdots \\
&= \frac{1+m_\pi/M}{1+m_\pi/M_d}\,(a_{\pi^- p}+a_{\pi^- n}) \\
&\quad +\; 2\frac{(1+m_\pi/M)^2}{1+m_\pi/M_d}\left[\left(\frac{(a_{\pi^- p}+a_{\pi^- n})}{2}\right)^2 - 2\left(\frac{(a_{\pi^- p}-a_{\pi^- n})}{2}\right)^2\right]\langle 1/r\rangle \\
&\quad +\cdots \\
&= 2\frac{1+m_\pi/M}{1+m_\pi/M_d}\,a^+ \\
&\quad +\; 2\frac{(1+m_\pi/M)^2}{1+m_\pi/M_d}\left[\left(\frac{a^+}{2}\right)^2 - 2\left(\frac{a^-}{2}\right)^2\right]\langle 1/r\rangle \\
&\quad +\cdots
\end{aligned}
\tag{4}
$$

Structure, multiple scattering and absorption effects are understood to be sufficiently under control [49, 50, 51, 56, 57, 58] and, consequently, $\Re\, a_{\pi d}$ *must* be expressible in terms of the elementary pion–nucleon amplitudes a^+ and a^-. Or vice versa, pionic deuterium yields a decisive constraint on the pionic hydrogen data.

In the limit of charge symmetry, pion absorption from the ground state in deuterium represents the inverse reaction of s-wave pion production $\pi^+ d \rightarrow pp$ at threshold. In both cases, the isospin $\Delta I = 1$ transition of the nucleon pair $({}^3S_1(I=0) \rightarrow {}^3P_1(I=1))$ is considered which has been found to dominate pion absorption at rest in the helium isotopes [59, 60]. The cross-section is parameterized by $\sigma(pp \rightarrow \pi^+ d) = \alpha C_0^2 \eta + \beta C_1^2 \eta^3$. The parameters α and β account for *s*- and *p*-wave production, respectively, $\eta = k_{\pi D}/M_\pi$ is the reduced momentum of the pion in the πD rest frame, and the factors C_i take into account the Coulomb interaction. Detailed balance relates α to the hadronic width in πD by $\Im\, a_{\pi D} = M_p\, \alpha \,/\, 6\pi$ [61].

Pion production in *pp* collisions is well studied at low energies. The average of the most recent data yield $\alpha \approx 215\,\mu\mathrm{b}$ [62, 63], which results in $\Im\, a_{\pi D} \approx (0.0037 \pm 0.0004)\, m_\pi^{-1}$. The result from the pionic deuterium width, corrected for $P_{\pi D}$, is $\Im\, a_{\pi D} = (0.0043 \pm 0.0005)\, m_\pi^{-1}$.

A first study in the approach of χPT including the next-to-leading order (NLO) terms yields $\alpha^{\mathrm{NLO}} \approx 220 \pm 70\,\mu\mathrm{b}$ [64]. The accuracy of the calculation is expected to improve by at least a factor of three within a few years [65]. Without the need of extrapolation to threshold the hadronic width of πD, to be significantly improved in the new πD experiment, provides the quantity α at the few per cent level.

4 Atomic Cascade in Pionic Hydrogen

Exotic atoms are formed when the kinetic energy of negatively charged particles like muons, pions or antiprotons are slowed down to a few eV. After capture by the Coulomb field of the nucleus into highly excited states a de-excitation cascade starts (Fig. 1). In atoms with $Z > 2$ the upper part of the cascade is dominated by Auger emission because the de-excitation rate depends on the energy difference $\Delta E_{nn'}$ between two levels n and n' by $\Gamma_{\mathrm{Auger}} \propto (1/\sqrt{\Delta E_{nn'}})$. In the lower part X-ray emission becomes more and more important owing to $\Gamma_{\mathrm{X}} \propto (\Delta E_{nn'})^3$. In the case of hadronic atoms the overlap of nuclear and atomic wave functions becomes significant and the occurrence of nuclear reactions from the low-lying states leads to level shifts and broadenings observable in X-ray transitions. A detailed discussion of the exotic-atom cascade may be found in [66].

In the case of a fully depleted electron shell already in the intermediate part X-ray emission dominates. Such a situation occurs for medium Z atoms when electron refilling is suppressed by using dilute targets [67, 68, 69]. This allows to use hydrogen-like exotic atoms as calibration standards in the few keV range because finite size effects are still negligibly small [70].

In $Z = 1$ exotic atoms, i. e., hydrogen, additional de-excitation processes play a decisive role. Because internal cascade processes proceed like $\Gamma_{\mathrm{X}} \propto Z^4$,

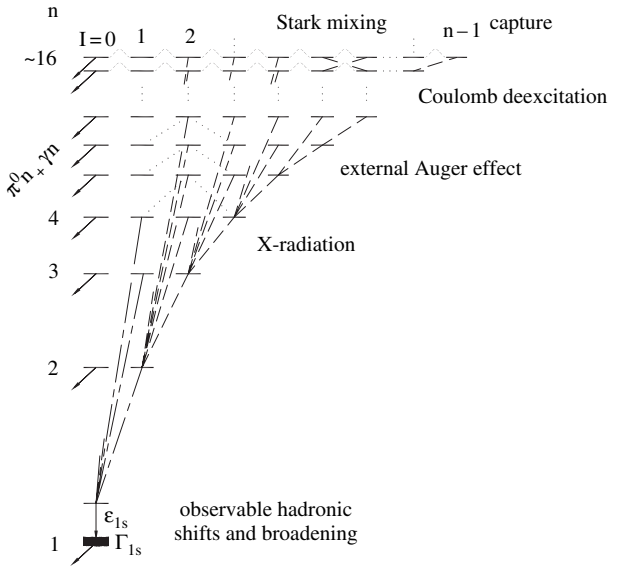

Fig. 1. Atomic cascade in pionic hydrogen. The transition energies of the $2p - 1s$, $3p - 1s$ and $4p - 1s$ X-rays are 2.4, 2.9 and 3.0 keV. The hadronic parameters ε_{ns} and Γ_{ns} scale with $1/n^3$. In case of pionic hydrogen, the s-wave interaction is attractive resulting in an increase of the binding energy ($\varepsilon_{1s} > 0$)

there is a frequent chance for collisions during the life time of the exotic system. In addition, exotic hydrogen is electrically neutral and, therefore, penetrates easily into other molecules of the target and experiences a strong Coulomb field there. Several processes competing during the cascade are briefly discussed below.

- *Stark mixing:* Within an electric field, to the pure parity states $|n\ell m\rangle$ admixtures are induced from states of the same principal quantum number n but different angular momentum according to the selection rules $\Delta\ell = \pm 1$ and $\Delta m = 0$ [71]. In the case of pions the induced low angular momentum leads to nuclear reactions already in high n states, which in turn depletes the cascade and reduces significantly the X-ray yields (Day–Snow–Sucher effect [72]). In the case of pionic hydrogen, only s-wave components experience the strong interaction.
- *Coulomb de-excitation:* The energy release for the de-excitation step $(\pi p)_{nl} \rightarrow (\pi p)_{n'l'}$ may be converted to a kinetic energy increase between the collision partners $\pi^- p$ and H (bound in an H_2 molecule). Coulomb de-excitation has been observed directly first by a Doppler broadening of time-of-flight distributions of neutrons from the two-body reaction $\pi^- p \rightarrow \pi^0 n$ [73]. Doppler contributions from several radiationless transitions $n \rightarrow n'$ were identified and kinetic energies up to 209 eV corresponding to 3–2 transitions have been seen both in liquid hydrogen and at a pressure of 40 bar. The acceleration increases (i) the collision probability and (ii) in the case of subsequent photon emission leads also to Doppler broadening of X-ray lines. As observed in the time-of-flight experiment, Coulomb transitions occur at any stage of the cascade, hence, a superposition of the various components is measured. Coulomb de-excitation even at lowest densities has been observed in muonic hydrogen μH [74]. There, however, no depletion of the cascade occurs by hadronic effects.
- *Inelastic and elastic scattering:* Between two radiationless transitions the velocity of the πH system is moderated by elastic and inelastic collisions, e. g., external Auger effect. For a precise determination of the hadronic width, the knowledge of the correction owing to the Doppler broadenings is indispensable. Important to mention, the Doppler broadening as measured by the neutrons may be composed very differently. The reaction $\pi^- p \rightarrow \pi^0 n$ takes place from ns states with mainly $n = 2$–5, whereas initial states $\pi H(np - 1s)$ X-ray transitions can be populated only by transitions from the outer part of the cascade.
- *Molecular formation:* As well established in muon-catalyzed fusion the collision of a μH atom with H_2 leads to resonant formation of complex molecules like $(\pi H)_{nl} + H_2 \rightarrow [(pp\pi)_{nvj}\ p]2e^-$ [75]. The quantum numbers v and j denote vibrational and total angular momentum of the 3-body molecular state. Similarly the 3-body system $(pp\pi)_{nvj}$ should be formed which is assumed to de-excite mainly by Auger emission [76, 77, 78]. But beforehand it cannot be excluded that a small fraction of a few per cent

of πH atoms bound into such molecules decays radiatively to the ground state. Decaying from molecular states small X-ray line shifts occur – always to lower energies – which cannot be resolved and, hence, could falsify the extracted hadronic shift. In the case of πD, it is predicted that the fraction of X-ray emission increases significantly [78]. However, it must be mentioned that metastable $2s$ states cannot occur for pions because of the nuclear reactions.

Besides small shifts due to the existence of molecular levels, Auger stabilization of $[(pp\pi)_{nvj}\ p]$ molecules is discussed. Again Auger transitions with lowest energy difference are preferred and satellites may occur a few eV below the line energy of the isolated system.

5 Experimental Approach

Both Coulomb de-excitation and molecule formation are scattering processes and, hence, depend on the collision rate, i. e., on density. Consequently, the strategy of the experiment was to study X-ray transitions at different densities. To be in addition sensitive to the initial state dependence of the maximal Doppler broadening, all πH transitions of sufficient line yield were also measured.

- The $\pi H(3p-1s)$ line (only in this case a suitable calibration line is available) was studied in the density range equivalent to 3.5 bar to liquid hydrogen, which corresponds to about 700 bar pressure.
- Information on Coulomb de-excitation is obtained by measuring besides the $\pi H(3p-1s)$ also the $\pi H(4p-1s)$ and the $\pi H(2p-1s)$ transitions. An increasing total line width with decreasing initial state must be expected because of the larger energy gain possible for the feeding transition, whereas the hadronic broadening is due to the $1s$ level only and therefore the same for all three lines.
- The measurement of the line width in muonic hydrogen allows the determination of the Doppler broadening without the necessity to subtract the hadronic line width. In this way a detailed comparison with predictions from cascade calculations on effects caused by Coulomb de-excitation becomes possible.

5.1 Set-Up at PSI

The new pionic hydrogen experiment is performed at the Paul Scherrer Institut (PSI, Switzerland). The experiment is set up at the high-intensity low-energy pion beam $\pi E5$ and consists of the cyclotron trap II, a cryogenic target, a reflection-type crystal spectrometer equipped with spherically bent crystals and a large-area CCD array for position-sensitive X-ray detection (Fig. 2). It is based on techniques developed and applied to the precision spectroscopy

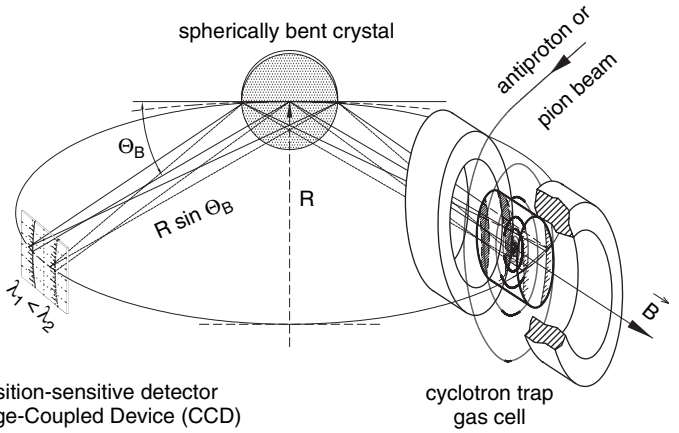

Fig. 2. Johann-type set-up of the Bragg spectrometer using the cyclotron trap to produce a high stop density for pions and a two-dimensional X-ray detector allowing the simultaneous measurement of an energy interval of several eV

of X-rays with the cyclotron trap I from antiprotonic and pionic atoms [22] together with substantial improvements in background suppression compared to the earlier πH experiments [79, 80].

The cyclotron trap, basically consisting of a superconducting split coil magnet, provides a concentrated X-ray source of suitable extension for a focusing low-energy Bragg spectrometer. Such a device is superior in stop density to a linear stop arrangement by two orders of magnitudes [81] and is indispensable because Stark mixing and hadronic reactions reduce the πH K X-ray line to a few per cent only [82].

After injection into the trap the beam is degraded by moderators in order to spiral into a gas cell positioned in the axis of the trap with a few revolutions only because of short pion life time. The wall of the gas cell is made of 50 µm thick kapton stabilized by a metallic frame and with a thin window of typically 7.5 µm mylar towards the crystal spectrometer. Higher densities than 1 bar of the target gases hydrogen and deuterium are established by cooling. At a pressure of 1 bar, about 0.5% of the incoming pions are stopped in the gas increasing linearly with density. In this experiment, cyclotron trap II has been used. Having a larger gap between the coils, one order of magnitude higher stop rates for muons could be achieved than for trap I. The muons are produced inside the trap from slow pions decaying close to the center of the magnet. Muon stop rates are typically 10% of the ones for pions.

X-rays emitted from the target gas are reflected by spherically bent silicon or quartz Bragg crystals of 10 cm diameter having a radius of curvature of about 3 m. To keep abberations (mainly from Johann broadening) small, the reflecting area is restricted to 60 mm horizontally. The spherical bending leads

to a partial vertical focusing, which increases the count rate. Typical Bragg angles are between 40° and 54°.

The X-rays are detected by a large-area two-dimensional position-sensitive detector built up from an array of six charge-coupled devices (CCDs) of type CCD22 with frame storage option [83]. Each CCD provides 600×600 pixels of 40 µm × 40 µm size yielding a total sensitive area of 48 mm×72 mm for the full array. With a depletion depth of about 30 µm the efficiency is maximal around 3.5 keV, ideally suited for the pionic and muonic X-rays having energies between 1.9 and 3.1 keV. The devices are cooled to –100°C and located inside a cryostat, which is separated from the spectrometer vacuum by an 5 µm thick aluminized mylar window.

An important feature when using CCDs as X-ray detectors is due to their two-dimensional sensitivity, the capability to analyze the hit pattern *and* having an energy resolution as good as high-performance Si(Li) detectors of typically 140 eV at 6 keV. At hadron machines, a high beam-induced background level is present from nuclear reactions. Such events, typically originating from Compton-induced processes, produce large structures. In comparison, the charge produced by few keV X-rays is collected in one or two pixels only. Together with massive concrete shielding (Fig. 3), a background reduction of more than two orders of magnitude is achieved, which is an decisive progress in view of exotic-atom X-ray rates of 20–100 per hour.

5.2 Energy Calibration

Johann-type spectrometers do not provide measurements of the absolute Bragg angle and, therefore, need a calibration line as close in energy as possible. The best choice is a narrow and intense transition in a hydrogen-like pionic atom not affected by strong interaction. In the case of pionic hydrogen the pair $\pi H(3p-1s)$ and $\pi O(6h-5g)$ fulfills these conditions. The large sensitive area of the X-ray detector allows the measurement of the $\pi H(3p-1s)$ transition and a calibration line without any change in the spectrometer set–up (Fig. 4 – left). This calibration method is basically free of systematic errors due to long-term instability. At higher densities hydrogen and oxygen have to be measured alternately to prevent the oxygen gas from freezing (Fig. 4 – right).

Fluorescence X-rays are much broader due to the large Auger width and may show satellite structures depending even on the excitation mechanism. Unfortunately, for the other πH lines considered as well as for πD no pionic lines are available. For pionic deuterium the fluorescence X-rays from gallium (measured in third order) and chlorine had to be used to determine the energy of the $\pi D(3p-1s)$ and $\pi D(2p-1s)$ transition, respectively. The accuracy is about a factor of 2 less compared to the exotic-atom case.

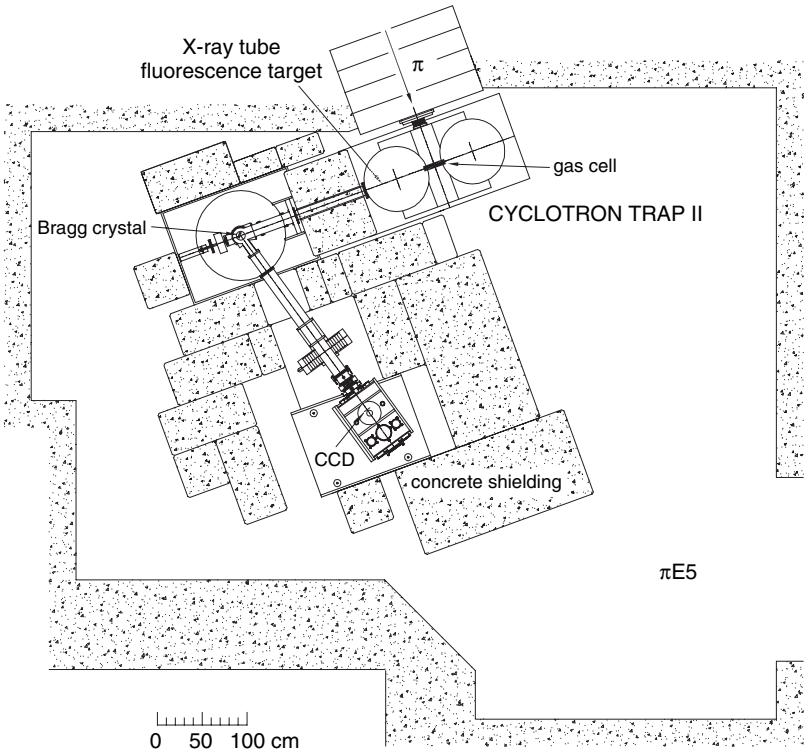

Fig. 3. Set-up for the pionic hydrogen experiment in the $\pi E5$ area at PSI. The concrete shielding of about 1 m thickness is essential to reduce the pion-induced background

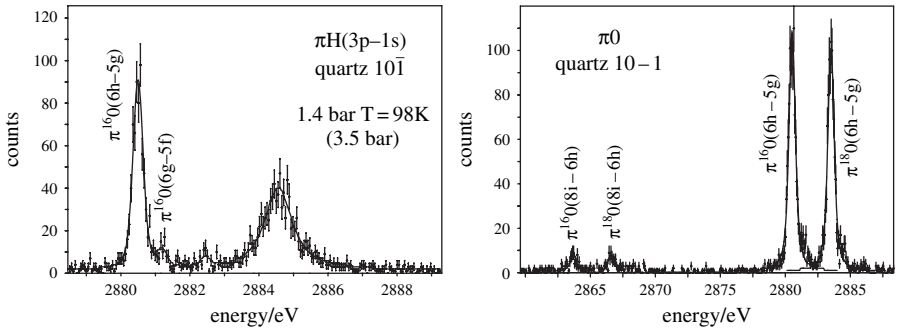

Fig. 4. Left: $\pi H(3p-1s)$ transition measured simultaneously with the $\pi O(6h-5g)$ transition by using an H_2/O_2 (90%/10%) gas mixture at an equivalent density of 3.5 bar. **Right**: $\pi O(6h-5g)$ transitions from the isotopes ^{16}O and ^{18}O. The energy splitting is used to verify the angular dispersion of the crystal spectrometer

5.3 Response Function

For the precise determination of the Lorentz contribution to the πH X-ray line shapes the knowledge of the crystal spectrometer response is required in detail. Because narrow fluorescence X-rays or few keV Γ lines for testing Bragg crystals are not available in practical cases, as a first approach narrow pionic-atom transitions were used [22, 80, 84]. Such lines have a natural width of a few tens of meV being negligible compared to the rocking curve width of silicon or quartz crystals of about 500 meV around 3 keV. Using CH_4 gas as target the experimental line shape was determined from the $\pi C(5g-4f)$ line, the energy of which is between the $\pi H(3p-1s)$ and $\pi H(4p-1s)$ transitions (Fig. 5 – left). In CH_4 a measurable Doppler broadening from Coulomb explosion is not expected, but cannot be completely excluded. The πC measurements reveal interesting cascade features by comparing the circular transition $\pi C(5g-4f)$ to the parallel transitions $\pi C(5f-4d)$ and $\pi C(5d-4p)$ and the $\pi C(5d-4p)$ line gives in addition access to the strong-interaction effects in the $4p$ states.

For a detailed measurement of the tails of the rocking curve the limited count rate, even at the high-flux pion channels, leads to unacceptable long measuring periods. Furthermore, a calibration line close to the $\pi H(2p-1s)$ transition at 2.4 keV is also desirable. Therefore, to allow an ultimate determination of the crystal properties, the technique of an Electron–Cyclotron-Resonance source has been used. In such a device few electron atoms are produced at high rates, in particular hydrogen- and helium-like systems which emit narrow X-ray lines because of the absence of Auger transitions.

The Electron–Cyclotron-Resonance Ion Trap (ECRIT), set up at PSI, uses the split coil magnet of the cyclotron trap to produce a bottle field with a high mirror ratio of about 4 [85]. A hexapole magnet is inserted in between the coils and the plasma is created by means of a 6.4 GHz high-frequency

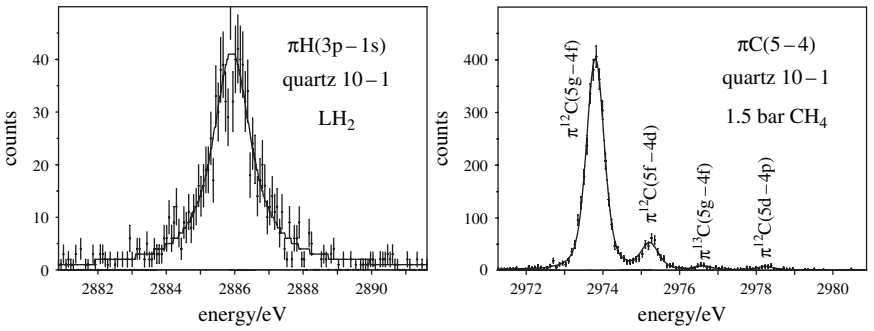

Fig. 5. Left: Preliminary determination of the crystal spectrometer response with the $\pi C(5g-4f)$ transition. The displayed spectra represent about 15% of the total width of the CCD array. **Right**: $\pi H(3p-1s)$ transitions as measured from liquid hydrogen

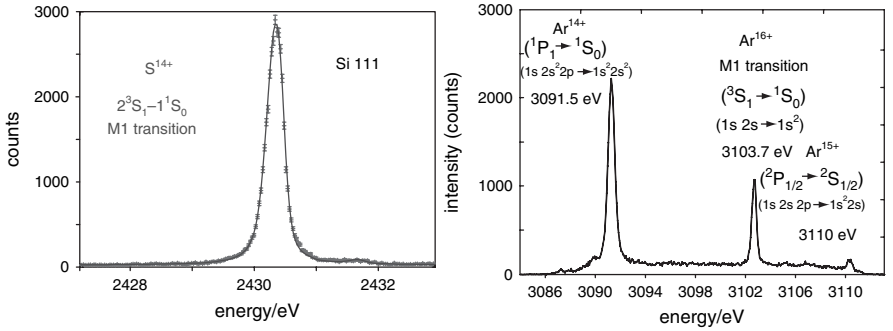

Fig. 6. Electronic X-rays from highly ionized sulfur and argon measured with a Si 111 crystal. The spectrometer response is determined from the M1 transition in He-like atoms

emitter. The crystal spectrometer was attached to one of the bore holes of the magnet. A cleaning magnet between ECRIT and Bragg crystal deflects the numerous electrons emitted on the magnet's axis in order to avoid a large background due to the scattered particles.

The plasmas were produced from sulfur, chlorine and argon, because for these elements the energies of the $2^3S_1 \rightarrow 1^1S_0$ M1 transitions coincide with the ones of the $\pi H(2p-1s)$, $\pi H(3p-1s)$ and $\pi H(4p-1s)$ lines. Count rates of up to 30000 per hour could be achieved allowing for a comprehensive diagnosis of the crystals (Fig. 6). In this way, focal lengths, the dependence of the resolution on apertures as well as the (asymmetric cut) angle between reflecting planes and surface could be determined precisely from the diffracted X-rays themselves [86]. A detailed study of X-ray emission from multiple charge states is in progress.

5.4 Muonic Hydrogen

The experimental response given, any additional broadening in muonic hydrogen transitions owes to Coulomb de-excitation. In Fig. 7 – left, the line shape of the $\mu H(3p-1s)$ line is compared to the resolution function as derived from the sulfur M1 transition.

Three components of the Doppler broadening are easily identified numerically by fitting the line shape. The kinetic energy distribution is modeled by four boxes adapted to cascade calculation (Fig. 7 – right) result with the relative weight being a free parameter in the fit. The two high energetic ones originating from Coulomb de-excitation between the states 5–4 and 4–3 are visible in the tails and as a kink at about 20% of the peak intensity, respectively. A low-energy component collects the transitions between higher states.

The spectrometer was set up in a way that an energy range of 10 eV to lower energies was accessible to allow the search for such satellite transitions stemming from Auger stabilization of molecule levels with subsequent X-ray

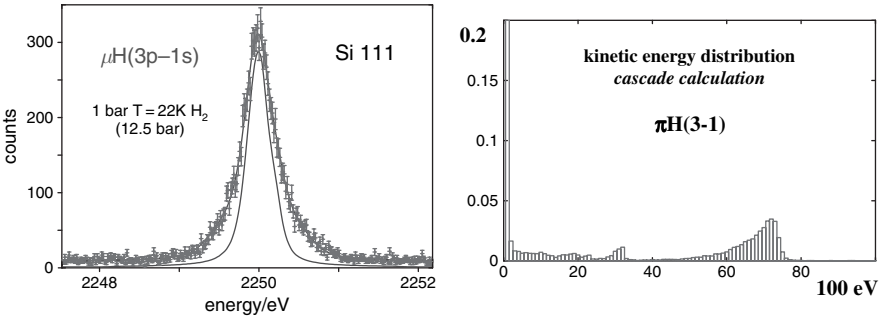

Fig. 7. Left: $\mu H(3p-1s)$ transition measured at an equivalent density of 10 bar. **Right**: Kinetic energy distribution as adapted from the cascade code of [88]. For fitting the measured $\pi H(3p-1s)$ spectrum the distribution was approximated by four Doppler boxes (0–2, 2–20, 29–33, 65–75) eV according to a low-energy component, (6–5), (5–4), (4–3) Coulomb transitions

de-excitation. No evidence was found for such nearby X-ray transitions from molecular states at the 1% level. This corroborates the findings from pionic hydrogen measurements where no pressure dependence of the Kβ transition energy could be identified.

As an additional result the fit to the line shape gives a triplet to singlet ratio of 2.96 ± 0.63 as expected from a statistical population of 3:1 for the $3p$ hyperfine levels. Leaving even the energy splitting as a free parameter the result is consistent with the calculated ground-state splitting of 183 meV [87].

6 Results

6.1 Transition Energy and Hadronic Shift

In pionic hydrogen, no density dependence was observed for the energy of the $\pi H(3p-1s)$ transition within the full density range of 3.5 bar to liquid [84] (Fig. 5 – right). It is concluded that the radiative decay of molecules is suppressed in hydrogen. The energy values obtained at all densities are consistent within the errors. A weighted average was calculated and compared to the pure electromagnetic $\pi H(3p-1s)$ transition energy calculated to $E^{\mathrm{QED}}_{3p-1s} = 2878.809 \pm 0.001$ eV [89]. The preliminary result for the shift in hydrogen of the new experiment (R–98.01) is

$$\varepsilon^{\pi H}_{1s} = 7120 \pm 11 \text{ meV}. \tag{5}$$

The error represents the quadratic sum of the statistical accuracy and all systematic effects, which originate from spectrometer set-up, imaging properties of extended Bragg crystals, analysis and instabilities. The contribution

from the uncertainty of the pion mass is negligible because the energy calibration was performed with the pionic-atom transition $\pi^{16}O(6h-5g)$. The new value for ε_{1s} is in good agreement with the result of the previous experiment (7.108 ± 0.036 eV), which used the cyclotron trap I and an energy calibration with argon Kα fluorescence X-rays [80].

For pionic deuterium, two earlier measurements of the transitions $\pi D(3p-1s)$ at 15 bar and $\pi D(2p-1s)$ at 2.5 bar pressure found $\varepsilon_{1s}^{\pi D} = -2.43 \pm 0.10$ eV [79] (energy calibration with Ar Kα) and $\varepsilon_{1s}^{\pi D} = -2.469 \pm 0.055$ eV [90] (Cl Kα). Both experiments are of limited statistics and small contributions from satellites due to molecular formation cannot be excluded. The $\pi D(3p-1s)$ experiment suffers in addition from a significant background level. The uncertainty of the $\pi D(2p-1s)$ line energy is dominated by the accuracy of the Cl Kα energy [91]. Therefore, a new high statistics measurement was performed recently, studying also the density dependence [24]. The analysis is in progress.

6.2 Line Width and Hadronic Broadening

For the $\pi H(2p-1s)$ line, a significant increase of the total width was found compared to the $\pi H(3p-1s)$ transition, which is explained by the higher energy release available from preceding transitions. Correspondingly, the $\pi H(4p-1s)$ line was found to be narrower [84] (Fig. 8 – left).

Already from the $\pi H(4p-1s)$ transition and using the $\pi C(5g-4f)$ line for the spectrometer response, an upper limit for $\Gamma_{1s} < 0.850$ eV can be determined. A more refined analysis using the ECRIT measurements corroborates this finding. To extract the hadronic width, the Doppler broadening was modeled by 2, 3 and 4 components for the $\pi H(4p-1s)$, $\pi H(3p-1s)$ and $\pi H(2p-1s)$ transitions. Very important is, due to the size of the detector, the possibility to cover fully the tails of the πH transitions. As important is a large enough region of background to the left and right.

The analyses of the three transitions $\pi H(2p-1s)$, $\pi H(3p-1s)$ and $\pi H(4p-1s)$ lines, treating the relative intensities of the Doppler broadening as free parameters, yield consistent values for the hadronic broadening

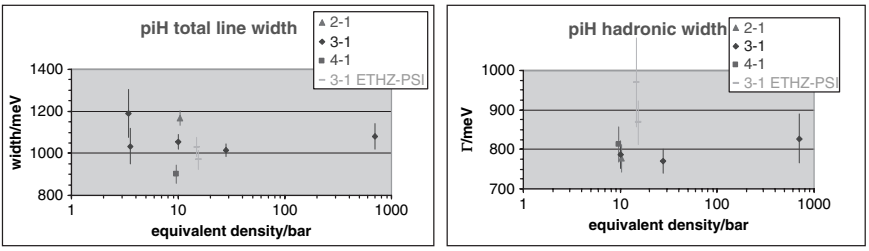

Fig. 8. Left: Total line width after subtraction of the spectrometer response only. **Right**: Hadronic width after subtraction of response and Doppler contributions

both for the various transitions and different densities (Fig. 8 – right). The averaged *preliminary* result of experiment *R*–98.01 is

$$\Gamma_{1s}^{\pi H} = 823 \pm 19 \ \text{meV} \tag{6}$$

consistent with the result of the previous experiment ($\Gamma_{1s} = 865 \pm 69$ meV [80]).

The hadronic width in pionic deuterium extracted first from the $\pi D(3p-1s)$ transition, $\Gamma_{1s}^{\pi D} = 1020 \pm 210$ meV [79], is in good agreement with the $\pi D(2p-1s)$ measurement yielding $\Gamma_{1s}^{\pi D} = 1093 \pm 129$ meV [90]. Due to limited statistics the fit is not sensitive to any Doppler contribution to the line width. The value given for $\pi D(2p-1s)$ line contains an estimate for the correction of 5 ± 5%. The resolution function was obtained here from a measurement of the $\pi^{20}\text{Ne}(7i-6h)$ line. In the new πD experiment a 20-fold higher statistics was collected and the ECRIT results are available for an ultimate description of the experimental response.

6.3 Scattering Length and Pion–Nucleon Coupling Constant

The shift ε_{1s} in πH yields the sum $a^+ + a^-$ of the isoscalar and isovector scattering lengths. In view of the precise experimental values, the accuracy is determined by the knowledge of the correction δ_ε (see Sect. 3). Within χPT $\delta_\varepsilon = (-7.2 \pm 2.9)\%$ [41] has been obtained. The uncertainty originates mainly from one particular LEC (f_1), which is practically unknown and dominates the uncertainty of a^+ (see Fig. 9). The result also obtained within χPT for the correction of the level broadening is reported to be $\delta_\Gamma = (0.6 \pm 0.2)\%$, [42]. Here, the LEC f_1 does not contribute and no significant uncertainty for the isovector scattering length a^- emerges from δ_Γ. An earlier approach for δ_ε and δ_Γ within a potential model ansatz led to $\delta_\varepsilon = (-2.1 \pm 0.5)\%$ and $\delta_\Gamma = (-1.3 \pm 0.5)\%$ [43] which, however, has been criticized to be incomplete.

As discussed earlier, any determination of a^+ from the hadronic shift in πD must be consistent with the values extracted from the πH results. Discrepancies have been reduced substantially by a recent calculation taking into account so-far neglected isospin breaking correction [55] (Fig. 9). Due to the smallness of a^+ these corrections amount to 42% in second order. The new and more precise measurement of $\varepsilon_{1s}^{\pi D}$ [24] will improve the constraints on a^+ and, in addition, for the electromagnetic LEC f_1, which appears in χPT calculations of charged pion scattering [39, 41, 55, 92].

Using the corrections calculated within χPT [41, 42], we obtain

$$a^+ = 0.0069 \pm 0.0031\, m_\pi^{-1}\,, \tag{7}$$

$$a^- = 0.0864 \pm 0.0012\, m_\pi^{-1}\,. \tag{8}$$

With the GMO sum rule analysis according to Ericson et al. [57], but inserting directly our value for a^- the πN coupling constant reads $f_{\pi NN}^2/4\pi = 0.076 \pm 0.001$ which yields $\Delta_{\text{GT}} = (1.98 \pm 0.02)\%$.

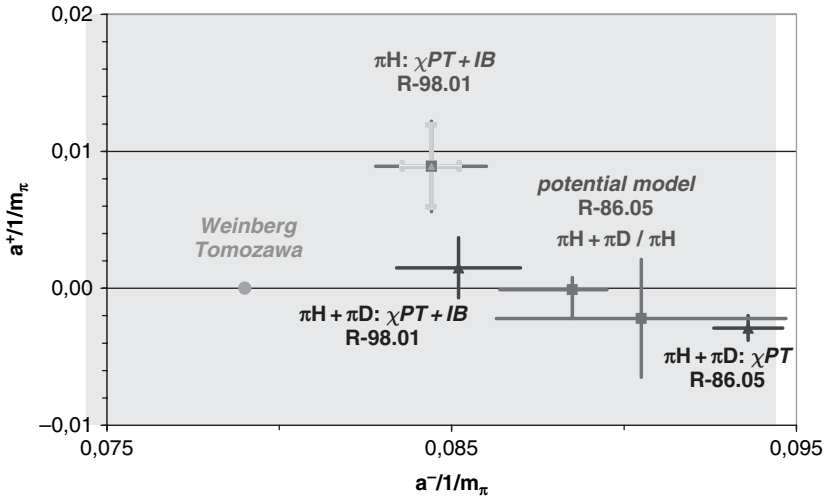

Fig. 9. Isoscalar and isovector πN scattering lengths a^+ and a^-. The results from this experiment ($R-98.1$) are obtained using δ_ε and δ_Γ as calculated within χPT [41, 42], whereas the previous experiment ($R-86.05$) applied the corrections determined in a potential approach [43]. Also given are the values from two analyses of the πH data together with $\varepsilon_{1s}^{\pi D}$ without ($\pi H + \pi D : \chi\mathrm{PT}$) and with ($\pi H + \pi D : \chi\mathrm{PT} + IB$) inclusion of isospin breaking corrections [54, 55]

An independent source for a^- is the photoproduction reaction $\gamma n \to \pi^- p$. The electric dipole amplitude is related to the isovector scattering length by $(a^-)^2 = (q/k_0) \cdot \mid E_{0+}^{\mathrm{thres}}(\pi^- p) \mid^2$, where q and k_0 are c.m.s. momenta of the photon and the pion [8]. With the result of Kovash et al., $E_{0+}^{\mathrm{thres}}(\pi^- p) = (-31.5 \pm 0.8) \cdot 10^{-3} m_\pi^{-1}$ [93], one obtains $a^- = 0.0842 \pm 0.022\, m_\pi^{-1}$. In turn a^- from πH yields a precise value $\mid E_{0+}^{\mathrm{thres}}(\pi^- p) \mid = (-32.5 \pm 0.4) \cdot 10^{-3} m_\pi^{-1}$ in good agreement with the prediction of χPT [94].

The hadronic width in pionic deuterium yields an imaginary part of the πd scattering length of $\Im\, a_{\pi D} = (0.0063 \pm 0.0007)\, m_\pi^{-1}$ [90]. Corrected for radiative capture the threshold parameter for pion production reads $\alpha = 250 \pm 30\,\mu\mathrm{b}$. An improvement by a factor of about 4 is expected from the new πD experiment to be compared with the continuously improving χPT calculations.

7 Summary and Outlook

A second series of high-precision experiments has been performed to determine strong interaction effects in pionic hydrogen and deuterium. A thorough study of the density dependence of X-ray energies and line widths together with a new method for an ultimate precision measurement of the crystal spectrometer response allows to a large extent the separation of atomic cascade and hadronic

effects resulting in an accuracy of about 1.5% for the πN scattering lengths. An extension to $A = 3$ systems may give additional clarification on how to build up light nuclei within the approach of χPT [95].

The accuracy in the determination of the πN scattering length concerning the presently available techniques have almost exploited their potentialities. Limitations now are mainly due to the understanding of the atomic cascade. First steps have been undertaken by including the development of the kinetic energies in order to develop a dynamical picture which is able to provide boundary conditions for the intensity of the components of the Doppler broadening [96, 97]. But up to now, the cross-sections used as input to such calculations do not allow a satisfactory description of the line shape measured in the $\mu H(3p-1s)$ experiment or the K-line intensities from high-lying states in πH. More detailed cross-section calculations are planned [98], and in particular the inclusion of molecular effects during the collisions seems to be needed.

References

1. S. Weinberg: Physica A **96**, 327 (1979).
2. W.-M. Yao et al. (PDG): J. Phys. G **33**, 1 (2006).
3. M. Gell-Mann, M. Lévy: Nuovo Cim. **16**, 705 (1960).
4. Y. Nambu: Phys. Rev. Lett. **4**, 380 (1960).
5. M. L. Goldberger, S. B. Treiman: Phys. Rev. **110**, 1478 (1958).
6. E. D. Commins, P. H. Bucksbaum: *Weak intercation of leptons and quarks* (Cambridge University Press 1983).
7. M. Gell-Mann, R. Oakes, and B. Renner: Phys. Rev. **122**, 2195 (1968).
8. T. E. O. Ericson and W. Weise: *Pions and Nuclei* (Clarendon, Oxford 1988).
9. A. W. Thomas, W. Weise: *The Structure of the Nucleon* (WILEY-VCH, Berlin 2001).
10. S. Scherer: 'Introduction to Chiral Perturbation Theory'. In: *Advances in Nuclear Physics* **27**, ed. by J. W. Negele, E. W. Vogt (Springer, 2003).
11. J. Gasser and H. Leutwyler: Ann. Phys. **158**, 142 (1984).
12. J. Gasser and H. Leutwyler: Nucl. Phys. B **250**, 465 (1985).
13. G. Ecker: Prog. Part. Nucl. Phys. **35**, 1 (1995), and references therein.
14. J. Gasser et al.: Phys. Rev. D**64**, 016008 (2001).
15. G. Colangelo, J. Gasser, and H. Leutwyler: Nucl. Phys. B **603**, 125 (2001).
16. B. Adeva et al.: Phys. Lett B **619**, 50 (2005).
17. CERN experiment PS212: http://dirac.web.cern.ch/DIRAC
18. E. Jenkins, A. V. Manohar: Phys. Lett. B **255**, 558 (1991).
19. V. Bernard, N. Kaiser, U.-G. Meissner: Int. J .Mod. Phys. E **4**, 193 (1995).
20. J. Gasser, H. Leutwyler, M. P. Locher, M. E. Sainio: Phys. Lett. B **213**, 85 (1988).
21. M. E. Sainio: 'Pion–nucleon σ-term – a review'. In: *Proc. of the 9^{th} Symp. on Meson–Nucleon Physics and the Structure of the Nucleon (MENU'01)*, *πN newsletter* **16**, 138 (2002), and references therein.
22. D. Gotta: Prog. Part. Nucl. Phys. **52**, 133 (2004).

23. PSI experiment R-98.01, http://pihydrogen.web.psi.ch.
24. PSI experiment R-06.03.
25. J. Spuller et al.: Phys. Lett. B **67**, 479 (1977).
26. S. Weinberg: Phys. Rev. Lett. **17**, 616 (1966).
27. Y. Tomozawa: Nuovo Cim. A, 707 (1966).
28. V. Bernard, N. Kaiser, U.-G. Meißner: Phys. Lett. B **309**, 421 (1993).
29. V. Bernard, N. Kaiser, U.-G. Meißner: Phys. Rev. C **52**, 2185 (1995).
30. V. Bernard, N. Kaiser, U.-G. Meißner: Nucl. Phys. A **615**, 483 (1997).
31. N. Fettes, U.-G. Meißner, S. Steininger: Nucl. Phys. A **640**, 199 (1998).
32. M. Mojžiš: Eur. Phys. J. C **2**, 181 (1998).
33. N. Fettes, U.-G. Meißner: Nucl. Phys. A **676**, 311 (2000).
34. N. Fettes, U.-G. Meißner: Nucl. Phys. A **693**, 693 (2001).
35. M. L. Goldberger, H. Miyazawa, and R. Oehme: Phys. Rev. **99**, 986 (1955).
36. V. L. Highland et al.: Nucl. Phys. A **365**, 333 (1981).
37. S. Deser, L. Goldberger, K. Kaufmann, and W. Thirring: Phys. Rev. **96**, 774 (1954).
38. G. Rasche and W. S. Woolcock: Nucl. Phys. A **381**, 405 (1982).
39. V. E. Lyubovitskij, A. Rusetsky: Phys. Lett. B **494**, 9 (2000).
40. V. E. Lyubovitskij, Th. Gutsche, A. Faessler, R. Vinh Mau: Phys. Lett. B **520**, 204 (2001).
41. J. Gasser et al.: Eur. Phys. J. C **26**, 13 (2002).
42. P. Zemp: In *Proc. of Chiral Dynamics 2003*, p. 128, Bonn, Germany, September 8–13 (2003), arXiv: hep–ph/0311212v1 and 'Pionic Hydrogen in QCD + QED: Decay Width at NNLO', Thesis univ. of Bern (2004).
43. D. Sigg et al.: Nucl. Phys. A **609**, 310 (1996).
44. T. E. O. Ericson, B. Loiseau, A. W. Thomas: Phys. Lett. B **595**, 76 (2004).
45. R. Koch: Nucl. Phys. A **448**, 1986 (1986).
46. *Proc. of MENU'01*, Washington, USA, πN newsletter **16**, (2002).
47. R. A. Arndt et al.: 'SAID phase shift analysis', http://gwdac.phys.gwu.edu.
48. T. L. Trueman: Nucl. Phys. **26**, 57 (1961).
49. S. R. Beane, V. Bernard, T.-S. Lee, U.-G. Meißner: Phys. Rev. C **57**, 424 (1998).
50. A. Deloff: Phys. Rev. C **64**, 065205 (2001).
51. S. R. Beane, V. Bernard, E. Epelbaum, U.-G. Meißner, D. R. Phillips: Nucl. Phys. A **720**, 399 (2003).
52. B. Burasoy, H. W. Grießhammer: Int. J. Mod. Phys. E **12**, 65 (2002).
53. M. Döring, E. Oset, M. J. Vicente Vacas: Phys. Rev. C **70**, 045203 (2004).
54. U. G. Meißner, U. Raha, A. Rusetski: Eur. Phys. J. C **41**, 213 (2005).
55. U.-G. Meißner, U. Raha, and A. Rusetski, Phys. Lett. B **639**, 478 (2006).
56. V. V. Baru, A. E. Kudryavtsev: Phys. of At. Nucl. **60**, 1475 (1997).
57. T. E. O. Ericson, B. Loiseau, A. W. Thomas: Phys. Rev. C **66**, 014005 (2002).
58. V. Lensky et al.: FZJ–IKP(TH)–2006–20, HISKP–TH–06–02, arXiv: nucl-th/0608042v1 (2006).
59. D. Gotta et al.: Phys. Rev. C **51**, 469 (1995).
60. E. Daum et al.: Nucl. Phys. A **589**, 553 (1995).
61. J. Hüfner: *Pions interact with Nuclei*, Phys. Rep. **21**, 1 (1975), formula (4.6).
62. P. Heimberg et al.: Phys. Rev. Lett. **78**, 1012 (1996).
63. M. Drochner et al.: Nucl. Phys. A **643**, 55 (1998).
64. V. Lensky et al.: Eur. Phys. J. A **27**, 37 (2006).
65. C. Hanhart: priv. comm.

66. In: *Proc. of the Fifth Course of the International School of Physics of Exotic Atoms*, ed. L. M. Simons, D. Horvâth, G. Torelli, Erice, Italy, May 14–20, 1989, (Plenum Press, New York 1990), and references therein.
67. R. Bacher et al.: Phys. Rev. Lett. **54**, 2087 (1985).
68. R. Bacher et al.: Phys. Rev. A **38**, 4395 (1988).
69. K. Kirch et al.: Phys. Rev. A **59**, 3375 (1999).
70. D. F. Anagnostopoulos, D. Gotta, P. Indelicato, L. M. Simons: Phys. Rev. Lett. **91**, 240801 (2003).
71. H. A. Bethe, E. E. Salpeter: *Handbuch der Physik*, Band **XXXV**, (Springer–Verlag, Berlin 1957).
72. T. B. Day, G. A. Snow, J. Sucher: Phys. Rev. Lett. **3**, 61 (1959); Phys. Rev. **118**, 864 (1960).
73. A. Badertscher et al.: Europhys. Lett. **54**, 313 (2001).
74. R. Pohl et al.: Phys. Rev. Lett. 97, 193402 (2006).
75. D. Taqqu: In *Muon Catalyzed Fusion*, AIP Conference Proceedings**181**, 217 (1989).
76. S. Jonsell, J. Wallenius, P. Froelich: Phys. Rev. A **59**, 3440 (1999).
77. E. Lindroth, J. Wallenius, S. Jonsell: Phys. Rev. A **68**, 032502 (2003).
78. S. Kilic, J.-P. Karr, L. Hilico: Phys. Rev. A **70**, 042506 (2004).
79. D. Chatellard et al.: Nucl. Phys. A **625**, 855 (1997).
80. H.-Ch. Schröder et al.: Eur. Phys. J. C **21**, 433 (2001).
81. L. M. Simons: Physica Scripta **T22**, 90 (1988); Hyperfine Int. **81**, 253 (1993).
82. A. J. Rusi El Hassani et al.: Z. Phys. A **351**, 113 (1995).
83. N. Nelms et al.: Nucl. Instr. Meth. A **484**, 419 (2002).
84. M. Hennebach: Precision Measurement of Ground State Transitions in Pionic Hydrogen. PhD Thesis, Universität zu Köln (2003).
85. S. Biri, L. M. Simons, D. Hitz: Rev. Sci. Instrum. **71**, 1116 (2000).
86. D. F. Anagnostopoulos et al.: Nucl. Instr. Meth. A **545**, 217 (2005).
87. R. N. Faustov, A. P. Martynenko: J. Exp. Theor. Phys. **98**, 39 (2004).
88. Th. Jensen: priv. comm.
89. P. Indelicato: priv. comm.
90. P. Hauser et al.: Phys. Rev. C **58**, R1869 (1998).
91. R. Deslattes et al.: Rev. Mod. Phys., **75**, 35 (2003).
92. U.-G. Meißner, S. Steininger: Phys. Lett. B **419**, 403 (1998).
93. M. A. Kovash et al.: πN Newsletter **12**, 51 (1997).
94. V. Bernard, N. Kaiser, U.-G. Meißner: Phys. Lett. B **383**, 116 (1996).
95. V. Baru, J. Haidenbauer, C. Hanhart, and J. A. Niskanen: Eur. Phys. J. A **16**, 437 (2003).
96. T. S. Jensen and V. E. Markushin: Eur. Phys. J. D **19**, 165 (2002); Eur. Phys. J. D **21**, 261 (2002); Eur. Phys. J. D **21**, 271 (2002).
97. T. S. Jensen: Eur. Phys. J. D **31**, 11 (2004) .
98. T. S. Jensen, V. Popov, V. Pomerantsev: priv. comm.